materials

MDPI

Article

Modelling of Longitudinal Elastic Wave Propagation in a Steel Rod Using the Discrete Element Method

Magdalena Knak [1,*], Michał Nitka [2], Erwin Wojtczak [1] and Magdalena Rucka [1]

[1] Department of Mechanics of Materials and Structures, Faculty of Civil and Environmental Engineering, Gdansk University of Technology, Narutowicza 11/12, 80-233 Gdansk, Poland; erwin.wojtczak@pg.edu.pl (E.W.); magdalena.rucka@pg.edu.pl (M.R.)

[2] Department of Buildings Structures and Material Engineering, Faculty of Civil and Environmental Engineering, Gdansk University of Technology, Narutowicza 11/12, 80-233 Gdansk, Poland; michal.nitka@pg.edu.pl

* Correspondence: magdalena.knak@pg.edu.pl

Abstract: The paper deals with the issue of modelling elastic wave propagation using the discrete element method (DEM). The case of a longitudinal wave in a rod with a circular cross-section was considered. A novel, complex algorithm consisting of the preparation of models and simulation of elastic waves was developed. A series of DEM models were prepared for simulations, differing in discretisation and material parameters. Additional calculations with the finite element method (FEM) were performed. Numerical wave signals were obtained from each simulation and compared with experimental results to choose the best DEM model based on the correlation between the waveforms. Moreover, dispersion curves were prepared for each model to verify the agreement with the Pochhammer-Chree wave propagation theory. Both experimental and theoretical approaches indicated the same model as the most suitable. The analysis results allowed stating that DEM can be successfully used for modelling wave propagation in structural rods.

Keywords: guided waves; longitudinal wave; discrete element method; finite element method; numerical modelling; dispersion curves

Citation: Knak, M.; Nitka, M.; Wojtczak, E.; Rucka, M. Modelling of Longitudinal Elastic Wave Propagation in a Steel Rod Using the Discrete Element Method. *Materials* **2022**, *15*, 2738. https://doi.org/10.3390/ma15082738

Academic Editor: Michele Brun

Received: 3 March 2022
Accepted: 6 April 2022
Published: 8 April 2022

1. Introduction

Ultrasonic guided waves are widely used in engineering structures' non-destructive testing (NDT). They are mostly applied to detect and localise damage [1–3] or determine elastic [4,5] and thermal properties [6–8]. For a comprehensive interpretation of results, experimental investigations can be enhanced with wave propagation simulations in numerical models. The calculations are typically performed in software implementing the finite element method (FEM). Modelling elastic wave propagation in the FEM is widely described in structural elements like rods and beams, plates and other more complex structures [3,9–11]. The FEM is mostly used for modelling structures made of homogeneous materials (e.g., isotropic steel or orthotropic composites). However, it can also be successfully applied in the case of highly heterogeneous materials (e.g., concrete). Several works consider the mesoscale structure of materials in terms of wave propagation [12,13]. For modelling and characterising the fracture properties of concrete, the discrete element method (DEM) is increasingly used, which allows for the study of its mechanical behaviour at the aggregate level. However, for discrete element-based techniques, the problem of wave propagation is not widely considered.

The discrete element method is a numerical modelling approach with many applications in various industries, e.g., hydromechanics, grinding, or even medicine [14–16]. The modelled structure is built from particles (mostly discs and spheres) that may interact with each other. For this reason, it is very popular in the fracture analysis of granular media such as sand [14–17] or concrete elements [18–26]. The geometry of the model, such as the

interactions between particles, are crucial issues. The DEM allows computing the motion of a large number of elements. Its main advantage is the high level of detail of the behaviour of each particle (at the macro- or even micro-level). The particles are considered perfectly rigid bodies but with smooth (soft) contacts (so-called overlaps). The DEM is based on the use of an explicit numerical integration scheme where the interaction of particles is monitored contact by contact. The motion of the particles is modelled one by one. It is based on Newton's second law, which is discretised by a finite difference shape, solved explicitly. In general, the DEM can be considered more complex than FEM, thus enabling an accurate reconstruction of the actual concrete mesostructure and a realistic prediction of fracture. An emerging research area is the investigation of the scattering of elastic waves within heterogeneous materials. However, the literature dealing with wave propagation problems in the DEM is still limited. An example of this kind of research was presented by Rojek et al. [27]. The authors described a micro-macro relationship in wave propagation simulation using the DEM. Their work involved calculations performed on 2D models using DEMPack software. The presented results confirmed the possibility of application of DEM for the simulation of guided wave propagation in solid materials.

The discrete element method is mainly used for modelling heterogeneous media. However, since concrete structures usually are reinforced by bars, reinforcement cannot be ignored in modelling, even though it is mostly made of steel. Thus, the current work is focused on the steel rod problem as the first step for further analysis directed to wave propagation-based diagnostics of reinforced concrete structures. The paper presents the guided wave propagation problem formulation in a circular rod using the DEM. A novel model preparation and calibration algorithm based on experimental and FEM analysis is developed. The main attention is paid to the process of the determination of discretisation and mechanical parameters.

The paper is structured as follows. The theoretical background of the DEM is given in Section 2, including basic formulae and computational methods. The proposed methodology for elastic wave modelling using the DEM is shown in Section 3. The description of the tested object with the details of experimental investigations and numerical calculations using the FEM and DEM methods is presented in Section 4. Moving on, Section 5 shows the results of the analyses performed. The guided waveforms obtained with the DEM were correlated with the experimental and FEM results. The theoretical dispersion curves were also incorporated to verify the proposed modelling algorithm. The paper completes in Section 6, which presents the main findings of the current study.

2. The Theoretical Background

2.1. Guided Waves in a Circular Rod

Longitudinal guided wave modes propagating in a circular rod with a radius r can be described by the Pochhammer-Chree frequency equation [28]:

$$\frac{2\alpha}{r}\left(\beta^2+k^2\right)J_1(\alpha r)J_1(\beta r)-\left(\beta^2-k^2\right)^2 J_0(\alpha r)J_1(\beta r)-4k^2\alpha\beta J_1(\alpha r)J_0(\beta r)=0, \quad (1)$$

where J_0 and J_1 stand for Bessel's functions of the first kind, parameters α and β are related to the wavenumber k, the angular frequency ω by:

$$\alpha^2=\frac{\omega^2}{c_P^2}-k^2,\ \beta^2=\frac{\omega^2}{c_S^2}-k^2 \quad (2)$$

In Equation (2), c_P^2 and c_S^2 denote the velocities of longitudinal and shear waves, respectively, and they are given by:

$$c_P=\sqrt{\frac{E(1-\nu)}{\rho(1+\nu)(1-2\nu)}},\ c_S=\sqrt{\frac{E}{2\rho(1+\nu)}} \quad (3)$$

where E is the young's modulus, ρ is the mass density and ν is the Poisson ratio. The solution of Equation (1) provides dispersion curves, which relate the group velocity to the angular frequency by the relation:

$$c_g = \frac{d\omega}{dk} \tag{4}$$

2.2. Outline of Discrete Element Method

The numerical analysis was performed with the open-source code Yade [29,30]. The algorithm for DEM calculations using spherical elements can be as follows. First, the position of every particle is established. Then, the contact between each particle and its neighbours (adjacent particles or other objects like walls or boxes) is found. If the contact exists, the overlap u is calculated from the equation:

$$u = d - (R_A + R_B), \tag{5}$$

where d is the distance between the centres of the elements and R_A and R_B are the radius of the elements in contact. Compression forces exist if the overlap is negative (if it is positive, tension appears).

The forces in contact points are calculated from the constitutive laws (Figure 1). This paper used the simple linear elastic (in compression) law. The equations are as follows:

$$\mathbf{F}_n = K_n u \mathbf{N}, \tag{6}$$

$$\mathbf{F}_s = \mathbf{F}_{s,prev} + K_s \Delta \mathbf{X}_s, \tag{7}$$

where, $\mathbf{F}_n$ and $\mathbf{F}_s$ are the normal and tangential contact forces, respectively (Figure 2), $\mathbf{N}$ is a unit normal vector on contact points connecting centres of the elements, $\mathbf{X}_s$ denotes the relative tangential displacement increment and $\mathbf{F}_{s,prev}$ is the tangential force calculated from the previous time step. Contact stiffnesses (i.e., normal stiffnesses K_n and tangential stiffnesses K_s) can be calculated from the following relations:

$$K_n = E_c \frac{2R_A R_B}{R_A + R_B}, \quad K_s = v_c E_c \frac{2R_A R_B}{R_A + R_B}, \tag{8}$$

where E_c is Young's modulus of particle contact and ν_c is the ratio between normal and tangential contact stiffness. For the normal (in tension) and tangential force, the limit is imposed:

$$F_s^{\max} = CR^2, \quad F_n^{\min} = TR^2, \tag{9}$$

where C corresponds to the cohesive contact stress (maximum shear stress at a pressure equal to zero) [29,31] and T to the normal tensile contact stress [29] (R is a minimum value of R_A and R_B). The current study's force values are relatively low (significantly lower than the limit); thus, contact break was not considered.

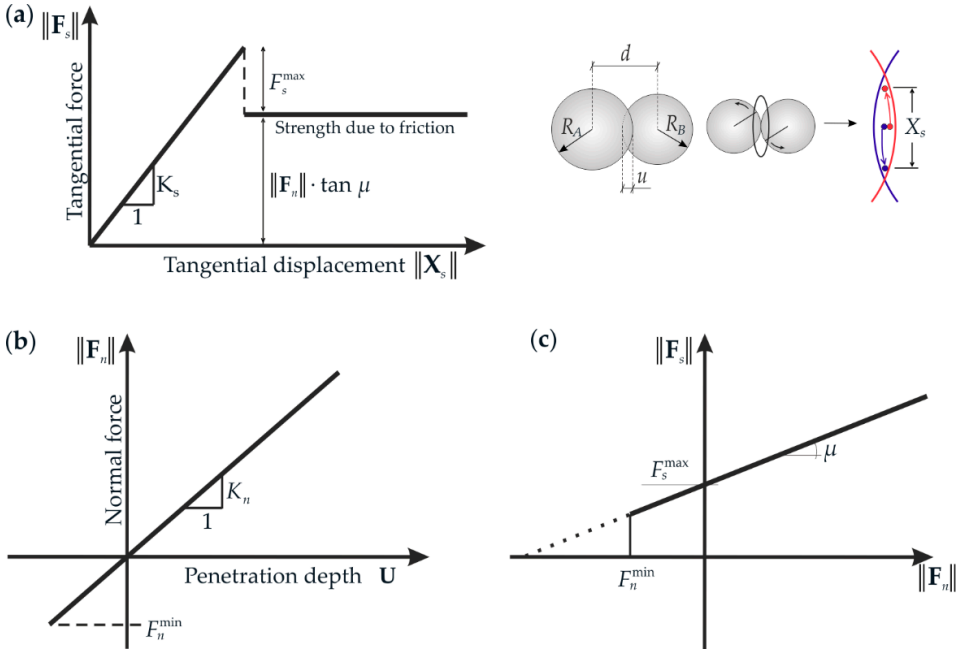

Figure 1. Mechanical response of DEM: (**a**) tangential contact model, (**b**) normal contact model, and (**c**) modified Mohr-Coulomb model [29].

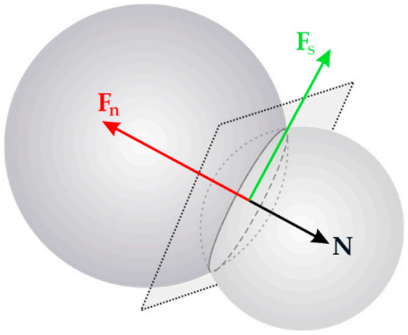

Figure 2. Two spheres in contact with the forces and momentum acting on them ($\mathbf{F}_n$—normal contact force, $\mathbf{F}_s$—tangential contact force, and **N**—normal contact vector) [29].

Moreover, the Coulomb friction is introduced. The model is described differently, depending on whether the contact is broken or not. The equations for the situation before and after the contact break can be expressed as follows, respectively:

$$\|\mathbf{F}_s\| - F_s^{max} - \|\mathbf{F}_n\| \tan\mu_c \leq 0, \tag{10}$$

$$\|\mathbf{F}_s\| - \|\mathbf{F}_n\| \tan\mu_c \leq 0, \tag{11}$$

where μ_c is the Coulomb inter-particle friction angle.

After force calculations, external forces (e.g., gravity or boundary conditions) may be added. In the next step, the motion of the elements is upgraded using Newton's second law. The acceleration, velocity, and finally, new particle position are calculated. Then, the first step is repeated. Note that in this paper, no damping is introduced (however, usually, for quasi-static calculations, it is necessary to use it). In the first step, the initial overlapping was calculated (u_{int}). Next, in every future step, Equation (6) was changed into:

$$\mathbf{F}_n = K_n(u - u_{\text{int}})\mathbf{N}. \tag{12}$$

So, the overlap can exist in the geometry; however, no initial forces are generated.

3. A Methodology of Building a DEM Model for Wave Propagation Problems

The simulation of the guided wave propagation phenomenon using the DEM is much more complex than in the FEM, even in the case of symmetric wave mode propagating in a rod with a circular cross-section. The current research proposes to build an appropriate model based on the calibration with experimental results. The methodology scheme developed using Yade software is presented in Figure 3. At first, it is assumed that the geometry of the rod (length l, diameter of the cross-section D), the density of the material ρ, and Young's modulus E are known (measured on the physical model). Some representative wave propagation signals need to be measured (using the particular excitation signal, e.g., wave packet). The first step of the scheme is the preparation of geometry, reflecting the physical model, including the length and cross-section of the rod. The discretisation with the use of spherical particles with the radius corresponding to the cross-section of the rod is required. The particles are arranged in a single line. An important parameter that must be assumed initially is the distance between the centres of the adjacent particles d. Furthermore, the number of adjacent particles with which a specific particle can interact can be set. It is determined by the parameter L_{int} specifying the area in which the centres of adjacent particles should be included to create an interaction. It is assumed that the specific particle should interact only with the closest neighbours (in general, two, one at each side); thus, the following condition needs to be satisfied:

$$d \leq L_{int} < 2d. \tag{13}$$

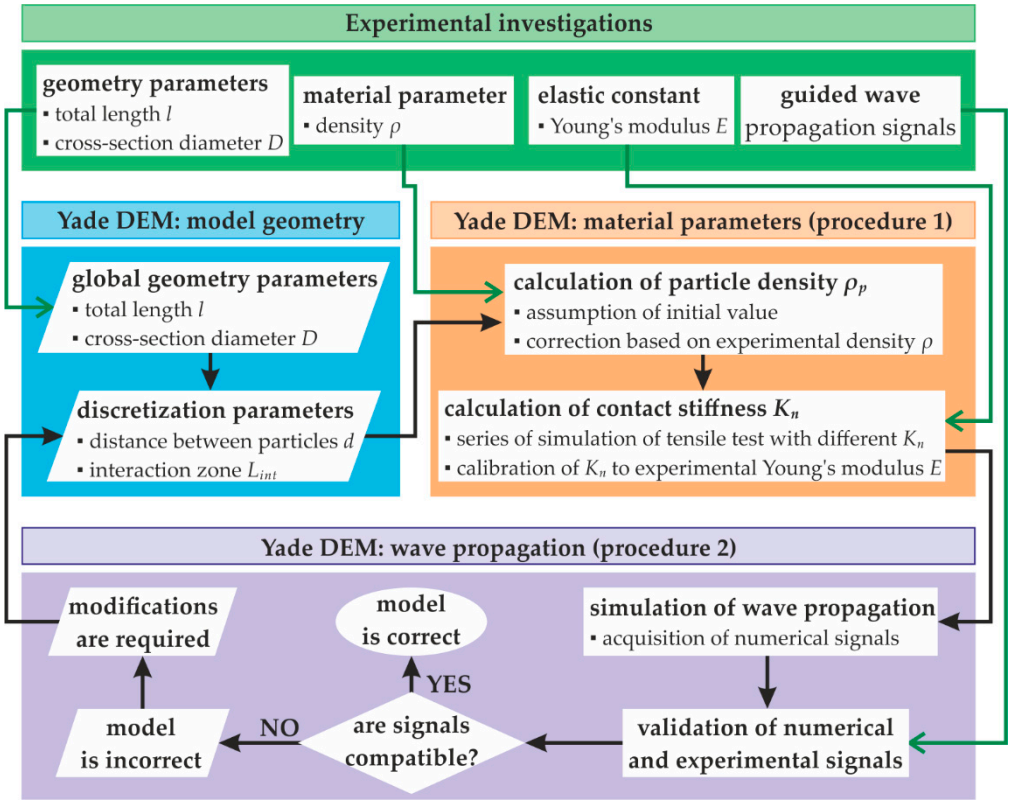

Figure 3. A scheme of building a DEM model of a rod with a circular cross-section for wave propagation using Yade DEM.

Having determined the model's geometry, the calculation of two crucial material parameters, i.e., the density of particles ρ_p and normal contact stiffness K_n needs to be performed using procedure 1 (as presented in Figure 3). First, the initial value of ρ_p is assumed. Based on this value, the total mass of the model is calculated and compared

with the actual mass of the physical model. The ratio between these two values is the correction coefficient that is further applied to the initial value of ρ_p to obtain the final particle density. When the value of ρ_p is established, a series of models with different values of K_n is prepared. A simple tensile test simulation is performed for each model to determine the stress-strain relation, also used to calculate Young's modulus E_{DEM}. The comparison between the series of E_{DEM} values and the experimental Young's modulus E allows for choosing the model with the appropriate contact stiffness. The resulting values of ρ_p and K_n, such as the geometry and discretisation previously established, are then incorporated into the second procedure concerning the wave propagation problem. The guided waves are excited and acquired. The signals obtained are compared with the experimental ones to validate the prepared model. The shape of waveforms, such as the wave velocity, can be verified, e.g., by determining the correlation between the two approaches. If the compatibility is satisfactory, the model is considered correct. If not, the model needs modifications, and the algorithm returns to the discretisation. The distance between particles must be changed, and the further steps in procedures 1 and 2 must be repeated. In the present case, if the wave velocity in the numerical signals is too low, the distance between particles needs to be decreased. Inversely, the distance should be increased if the velocity is too high. In general, multiple repetitions of the steps presented can be required.

4. Materials and Methods

4.1. Object of Research

The object of the investigation (Figure 4a) was a rod with a circular cross-section (diameter D = 10.2 mm) and a length of l = 1000 mm. The rod was made of steel, with the following material parameters: mass density ρ = 7850.66 kg/m^3, Young's modulus E = 208.72 GPa (determined in a static tensile test) and Poisson's ratio ν = 0.3.

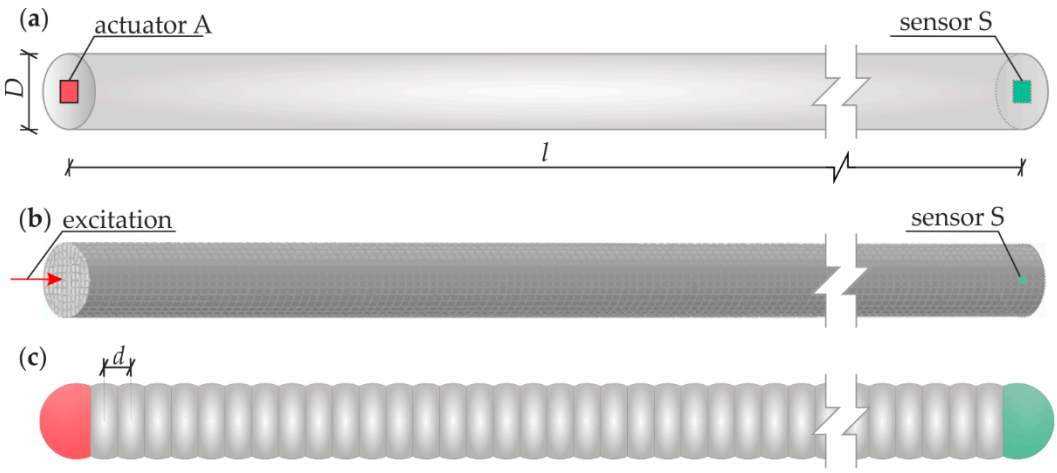

Figure 4. An object of research: (**a**) specimen geometry, (**b**) numerical FEM model, (**c**) numerical DEM model.

4.2. Experimental Procedure

The experimental measurements of guided waves were carried out using piezoelectric plate transducers Noliac NAC2011 with dimensions of 2 × 2 × 2 mm^3. One of the transducers acted as an actuator (A), while the second (S) acted as a sensor. The actuator was attached to one end of the rod, while sensor S was attached to the other end, as shown in Figure 5a, so the waves were excited and sensed in the longitudinal direction. The wave packet induced by the actuator was a five-cycle sine function modulated with a Hann window (Figure 5b). The central frequency of the wave packet was set in the frequency range of 50–150 kHz with a step of 10 kHz. Signals were further processed with the Hilbert transform to obtain signal envelopes [32].

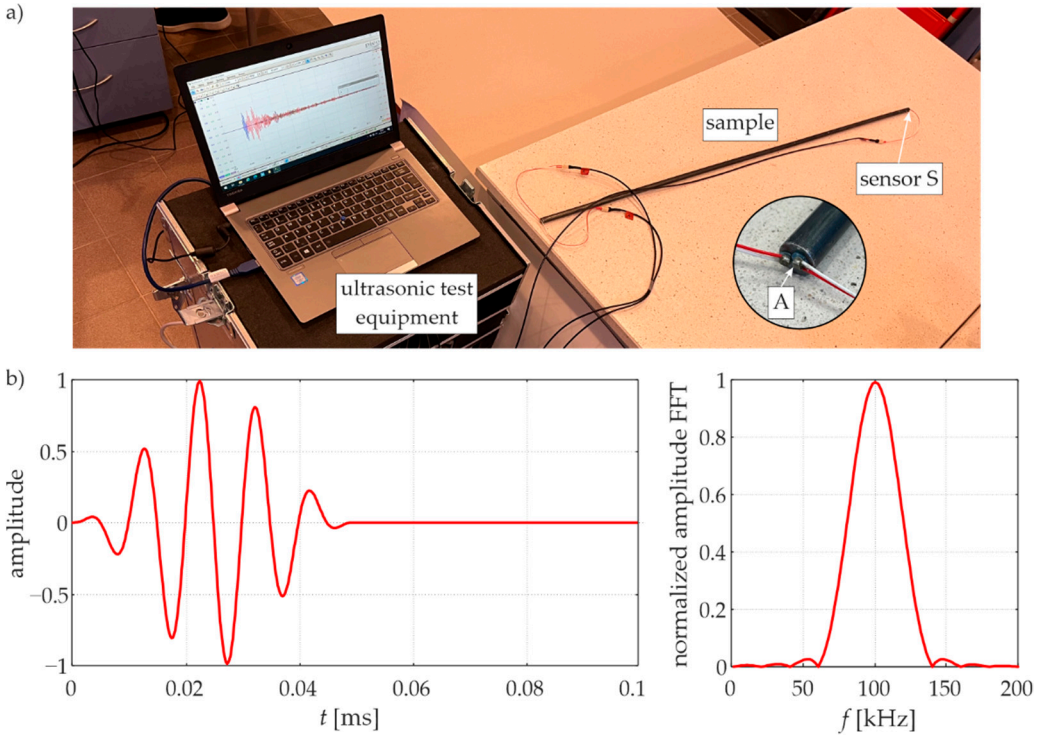

Figure 5. (**a**) Experimental setup. (**b**) Five-cycle sine wave packet with the carrier frequency of 100 kHz (time-domain signal and frequency spectrum).

4.3. Numerical Modelling

4.3.1. Finite Element Method

Numerical analysis was performed in the Abaqus software based on the finite element method. The created 3D model of a bar (Figure 4b) reflected the experimental object (including geometry and mechanical parameters). A linear-elastic, homogeneous, isotropic material model was used. Rayleigh proportional damping was assumed with a mass proportionality coefficient equal to α = 2000 1/N, neglecting the influence of stiffness (β = 0 m/N). The use of damping allows one to reflect the real wave propagation in the tested object. Boundary conditions were assumed as free edges. The numerical model was made of solid 8-node finite elements with reduced integration (C3D8R). The mesh grid had a size of $1 \times 1 \times 1$ mm^3. The explicit module was used to calculate the guided waves propagation problem. An algorithm of the central difference method has been applied to integrate the equation of motion. The total calculation time was assumed to be 1.5 ms with the time step equal to $1 \cdot 10^{-7}$ s. The wave was excited by applying a concentrated force of a certain amplitude at one end of the rod. The input signal was the same as in the experimental investigations. The results of the analysis were recorded at the point at the opposite end.

4.3.2. Discrete Element Method

Numerical calculations based on the discrete element method were performed in the Yade environment. There are a few significant parameters in wave propagation calculations: the particle density ρ_p, normal contact stiffness K_n, the geometry (initial distance between the spheres d) and the coordination number (the number of contacts for every element, determined by the interaction zone L_{int}). In the first step, samples with a predetermined geometry were prepared. The steel bar was created as a 3D model as one row of spherical elements with a length of l = 1000 mm (Figure 4c). The radius of each particle was constant and equal to half the diameter of the real bar (R = 5.1 mm). The parameter of the initial distance of the particle d has been changed. The interaction zone L_{int} was chosen so that the specific particle interacted only with its nearest neighbours. For such prepared

geometry, the quasi-static tension test was performed (only elastic part, with no breakage). The density parameter was unique for a specified distance to keep the overall mass of the bar in agreement with the real value. The modification of the stiffness coefficient directly affects the global Young's modulus E_{DEM}. The prepared model was used for the 1D problem of longitudinal wave propagation. An explicit procedure was used, and the time step equal to $dt = 5 \times 10^{-8}$ s was adopted (critical time step $dt_{cr} = 1.3 \times 10^{-5}$ s). The total computation time was 1.5 ms. No additional damping was applied to the model; nevertheless, attenuation was observed in the signals (resulting from the geometrical damping). The disturbance was induced by force applied to the first particle. The signal was recorded at the last particle (at the end of the bar, sensor S).

5. Results

A series of calculations were carried out to calibrate the DEM numerical model with the experiment. In the following steps, due to the size of the calculation, only the results for selected particle distances $d = \{0.95R, 1.03R, 1.05R, 1.15R\}$ are presented. This set was chosen to show all aspects of the considered issue and the arising difficulties as clearly as possible. The experimental signal was taken as a reference one, to which the numerical signals were matched. The adjustment accuracy was determined qualitatively by visual evaluation of the signals and quantitatively using the Pearson correlation coefficient (PCC), such as the sum of squared errors of the longitudinal wave velocities.

The first step of the calculation for each different distance was to determine the static parameter (Young's modulus). The static tensile test simulation was performed for different values of contact stiffness K_n (assumed heuristically). Young's modulus E_{DEM} was determined for each calculation by linear approximation of the stress-strain relation obtained from the measurements. The final value of the contact stiffness K_n corresponded to the model with an E_{DEM} value close to the real value of E. Figure 6 presents an example of the stress-strain relationship and its approximation for the model with $d = 1.03R$.

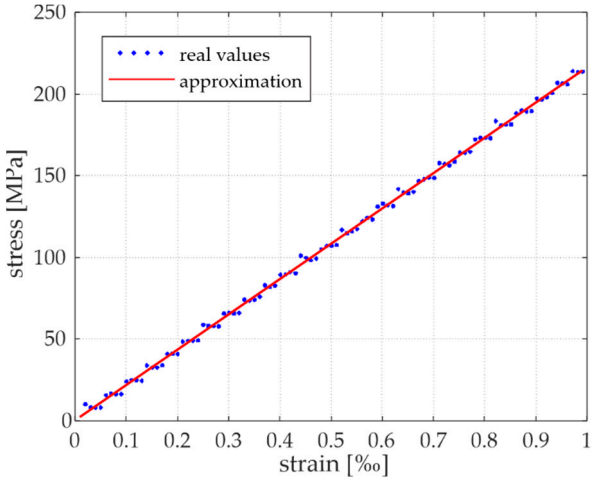

Figure 6. Stress-strain relation for the $1.03R$ model for the determination of K_n.

Having determined all the appropriate parameters, the guided wave propagation calculations were carried out. Figure 7 shows the signals of the longitudinal wave collected at the sensor. The signals for four selected distances of particles ($d = \{0.95R, 1.03R, 1.05R, 1.15R\}$) are presented. Excitation frequencies equal to 50 kHz, 100 kHz, and 150 kHz were analysed. Firstly, there is a decrease in velocity with increasing frequency. When considering the models' signals with different particle distances, it is evident that the $d = 0.95R$ strongly deviates from the others. The densification of the rod particles implies an increase in the propagation speed of the wave. Moreover, a numerical dispersion is much more pronounced (in comparison to the three other models) at higher frequencies.

When comparing the waveforms presented, it can be concluded that the 0.95R model is the most unstable.

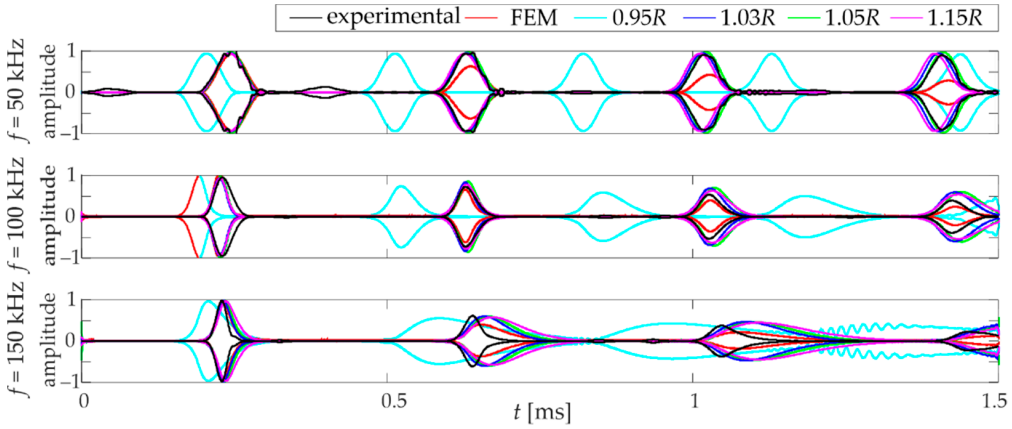

Figure 7. Comparison of signal for selected DEM models (various overlap) and frequencies.

Correlation calculations were performed using the PCC to determine which model is the most unambiguously compatible with the experiment. Table 1 shows the estimated static parameters for selected models with different particle distances with correlation coefficients. The comparison is intended to show the influence of the agreement distance parameter on the obtained agreement with reference (experimental) measurements and FEM calculations. A strong effect of the distance applied in the DEM model on the obtained correlation can be observed. This confirms previous observations, that the signals received for $d = \{1.03R, 1.05R, 1.15R\}$ are comparable. Their average correlation coefficients (for all particular frequencies) indicate high similarity. However, this requires verification over a wider frequency range.

Table 1. Properties of DEM models.

Model	Number of Particles	Density ρ_p (kg/m^3)	Normal Contact Stiffness K_n (N/m)	Young's Modulus E_{DEM} (GPa)	Correlation with Experiment PCC	Correlation with FEM PCC
0.95R	207	5577.17	2.3×10^{11}	207.30	−0.018	−0.012
1.03R	191	6044.37	6.6×10^{11}	216.30	0.906	0.892
1.05R	187	6173.66	6.4×10^{11}	213.97	0.862	0.886
1.15R	171	6751.31	6×10^{11}	219.37	0.853	0.860

Figure 8 presents the PCC variation in relation to the wave frequency. The correlation between numerical (FEM and DEM with different overlaps) and experimental waveforms are shown in Figure 8a. First, it can be observed that there is a rapid decrease in the PCC at higher frequencies. The decrease is related to the presence of an increasing numerical dispersion. A good agreement between the experimental and FEM results can be observed (PCC above 0.85). In the case of DEM results, the PCC is above 0.7 only for the 1.03R model; it could be considered a strong correlation [33]. When the experimental vs. DEM correlation curves are considered, a characteristic decrease in the PCC value is observed with an increase in the distance between the particles. Furthermore, it can be seen that in the frequency range of 50–90 kHz, the PCC values of DEM vs. experimental signals are noticeably higher than the PCC values of FEM vs. experimental signals, but above a frequency of 100 kHz FEM model gives a stronger correlation. Figure 8b illustrates a plot of the PCC calculated between the FEM and DEM signal envelopes. A strong agreement between the methods is shown within the analysed frequencies. The PCC for all models

ranges between 0.8 and 1.0. This confirms that these two different numerical approaches can give comparable results.

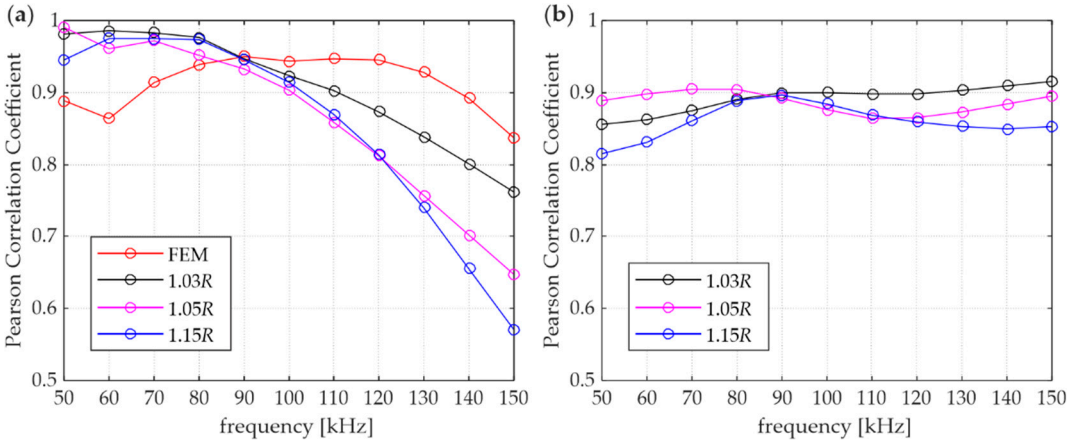

Figure 8. Pearson correlation coefficient in relation to excitation frequency: (**a**) FEM and DEM vs. experimental results, (**b**) DEM vs. FEM results.

For wave propagation analysis, it is crucial to recognise the relationship between velocity and frequency. Thus, the characteristic dispersion curves were determined for the steel bar analysed. Theoretical curves were obtained using PCDISP software based on the Pochhammer-Chree theory [34,35]. The numerical FEM/DEM curves were obtained by calculating wave propagation velocity based on two adjacent wave packets using the 'peak to peak' method. Figure 9 shows the dispersion curves obtained by different approaches. The DEM curves for four different distances were compared with the theoretical ones. This comparison is intended to highlight the accuracy of the adopted discrete model. First of all, it is worth noting that the obtained curves indicate the dispersive nature of the waves in DEM. Second, it can be pointed out that the group velocity is closely related to the applied particle distance. The shorter the distances between the particle's centres, the faster the wave propagates. As the distance increases, the group velocity decreases. Additionally, as the frequency increases, the velocity decreases. In the case of $d = 1.05R$ and $d = 1.15R$, the curves that fit the theoretical curve at lower frequencies start to deviate increasingly from the theory as the frequency increases. The dispersion curve obtained for the DEM model at $d = 1.03R$ was selected to present the greatest agreement with the theory and the numerical FEM result (the group velocity of the numerical FEM is in accordance with the theoretical one at all frequencies). To determine the degree of similarity and confirm the proposed solution's validity, the residual sum of squares (RSS) was calculated [5]. The results obtained are summarised in Table 2. The RSS values clearly show the agreement of the applied models. Analysing the values for the numerical DEM models, it can be observed that the best agreement (the lowest value of RSS) is shown for the $d = 1.03R$ model.

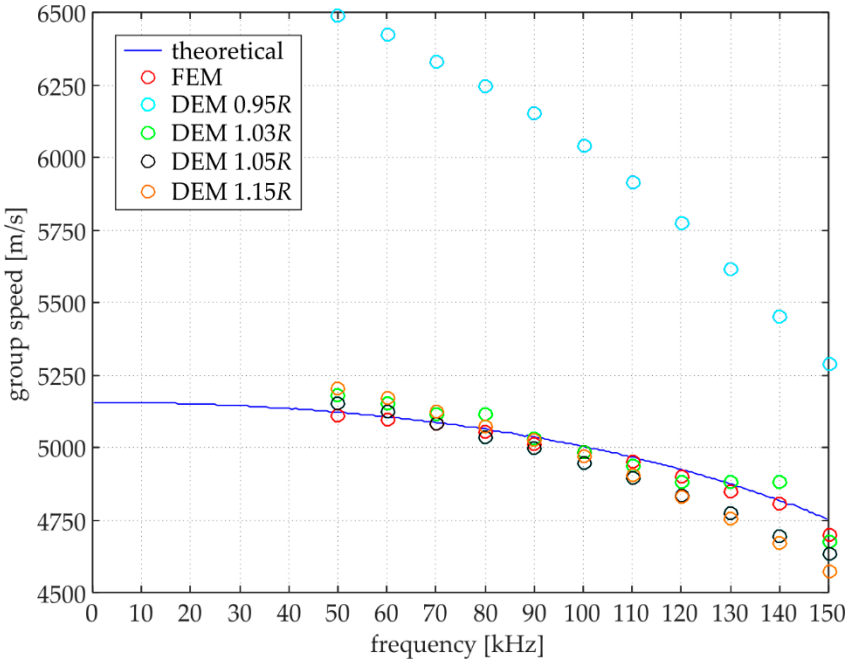

Figure 9. Comparison between dispersion curves for numerical models and Pochhamer-Chree theory.

Table 2. Residual sum of squares between numerical models and Pochhammer-Chree theory.

Model	RSS
FEM	6056
DEM, 0.95*R*	11,694,645
DEM, 1.03*R*	22,436
DEM, 1.05*R*	61,084

The wave propagation results for the final DEM model (d = 1.03R) are shown in Figure 10. The experimental results are compared with the numerical results obtained from FEM and DEM calculations. By analysing the graphs, it is possible to observe the compatibility of the speed of wave propagation and the compatibility of the shape of the wave packets. The first wave packets that appear are compatible with each other. The satisfactory compatibility of guided wave calculations was achieved using the discrete element and finite element methods. As mentioned earlier, the superiority of DEM over FEM can be seen at lower frequencies (50–90 kHz). The packet shapes obtained in the DEM calculations reflect the experimental ones clearly enhanced. A characteristic effect of dispersion is seen in both numerical models at higher frequencies. There is an elongation of the numerical packets, while their beginnings are consistent with the experimental ones.

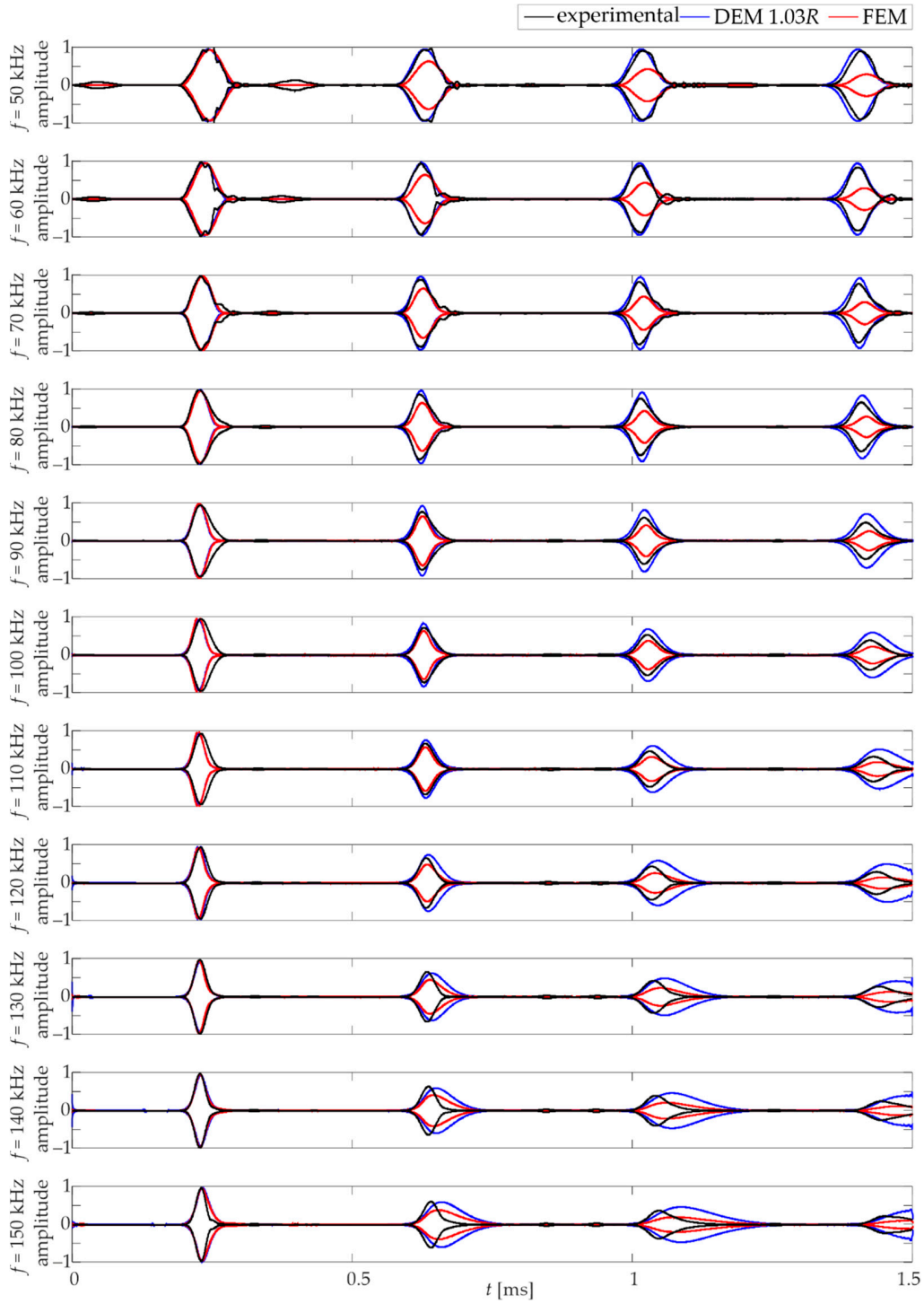

Figure 10. Comparison of wave propagation for experimental and numerical FEM/DEM results.

6. Conclusions

The paper describes the modelling of longitudinal wave propagation in a circular steel rod using the discrete element method. An experimental approach was applied to verify the appropriateness of DEM modelling in the Yade open-source code. The finite element calculations performed in Abaqus software supported the performed analyses. Based on the results, the following conclusions could be formulated.

- The Yade platform can be successfully used for experimentally assisted guided wave modelling. The geometric and material parameters need to be determined on a

physical model. Moreover, measurements of a certain number of wave propagation signals are required.

- The heuristic process is the appropriate choice of parameters used in DEM models (distance between particles and contact stiffness). The DEM allows one to create several discrete models that fit the experimental results for different sets of parameters. However, further analyses, e.g., dispersion curve calculation, enable selecting the most suitable model.
- Dispersion curves confirmed that guided waves in DEM exhibit a dispersive nature. There is a visible change in group velocity in relation to frequency. Moreover, the wave velocity is closely related to the particle distribution, i.e., the smaller the distances between particles, the higher the group velocity.

In summary, it can be concluded that the discrete element environment can be successfully used for wave propagation analysis. The present work is a beginning consideration for more complex problems, especially to explain the mechanism of propagation and scattering of elastic waves in concrete members at the aggregate level. In the next steps, the calibration of waveforms in concrete and reinforced concrete elements using DEM will be performed.

Author Contributions: Conceptualization, M.K., M.N., E.W. and M.R.; methodology, M.K., M.N., E.W. and M.R.; numerical investigation, M.K. and M.N., experimental investigation, M.K., E.W. and M.R.; software, M.K. and M.N.; formal analysis, M.K., M.N. and E.W.; writing—original draft preparation, M.K., M.N. and E.W.; writing—review and editing, M.R.; visualization, M.K. and E.W.; supervision, M.R. All authors have read and agreed to the published version of the manuscript.

Funding: This research received no external funding.

Institutional Review Board Statement: Not applicable.

Informed Consent Statement: Not applicable.

Data Availability Statement: The data underlying this article will be shared on reasonable request by the corresponding author.

Conflicts of Interest: The authors declare no conflict of interest.

References

1. Mitra, M.; Gopalakrishnan, S. Guided wave based structural health monitoring: A review. *Smart Mater. Struct.* **2016**, *25*, 53001. [CrossRef]
2. Song, H.; Popovics, J.S. Characterization of steel-concrete interface bonding conditions using attenuation characteristics of guided waves. *Cem. Concr. Compos.* **2017**, *83*, 111–124. [CrossRef]
3. Wojtczak, E.; Rucka, M.; Knak, M. Detection and Imaging of Debonding in Adhesive Joints of Concrete Beams Strengthened with Steel Plates Using Guided Waves and Weighted Root Mean Square. *Materials* **2020**, *13*, 2167. [CrossRef]
4. Cui, R.; Lanza di Scalea, F. On the identification of the elastic properties of composites by ultrasonic guided waves and optimization algorithm. *Compos. Struct.* **2019**, *223*, 110969. [CrossRef]
5. Wojtczak, E.; Rucka, M. Monitoring the curing process of epoxy adhesive using ultrasound and Lamb wave dispersion curves. *Mech. Syst. Signal Process.* **2021**, *151*, 107397. [CrossRef]
6. Tiwari, R.; Mukhopadhyay, S. Boundary Integral Equations Formulation for Fractional Order Thermoelasticity. *Comput. Methods Sci. Technol.* **2014**, *20*, 49–58. [CrossRef]
7. Tiwari, R.; Kumar, R.; Kumar, A. Investigation of thermal excitation induced by laser pulses and thermal shock in the half space medium with variable thermal conductivity. *Waves Random Complex Media* **2020**, 1–19. [CrossRef]
8. Tiwari, R.; Kumar, R. Analysis of plane wave propagation under the purview of three phase lag theory of thermoelasticity with non-local effect. *Eur. J. Mech. A/Solids* **2021**, *88*, 104235. [CrossRef]
9. Moser, F.; Jacobs, L.J.; Qu, J. Modeling elastic wave propagation in waveguides with the finite element method. *NDT E Int.* **1999**, *32*, 225–234. [CrossRef]
10. Yang, C.; Ye, L.; Su, Z.; Bannister, M. Some aspects of numerical simulation for Lamb wave propagation in composite laminates. *Compos. Struct.* **2006**, *75*, 267–275. [CrossRef]
11. Wojtczak, E.; Rucka, M. Wave frequency effects on damage imaging in adhesive joints using lamb waves and RMS. *Materials* **2019**, *12*, 1842. [CrossRef] [PubMed]
12. Chen, H.; Xu, B.; Wang, J.; Luan, L.; Zhou, T.; Nie, X.; Mo, Y.L. Interfacial debonding detection for rectangular cfst using the masw method and its physical mechanism analysis at the meso-level. *Sensors* **2019**, *19*, 2778. [CrossRef] [PubMed]

13. Xu, B.; Chen, H.; Mo, Y.L.; Zhou, T. Dominance of debonding defect of CFST on PZT sensor response considering the meso-scale structure of concrete with multi-scale simulation. *Mech. Syst. Signal Process.* **2018**, *107*, 515–528. [CrossRef]
14. Thornton, C.; Yin, K.K.; Adams, M.J. Numerical simulation of the impact fracture and fragmentation of agglomerates. *J. Phys. D Appl. Phys.* **1996**, *29*, 424–435. [CrossRef]
15. Herrmann, H.J.; Luding, S. Review Article: Modeling granular media with the computer. *Cont. Mech. Ther.* **1998**, *10*, 189–231. [CrossRef]
16. Jiang, M.J.; Yu, H.S.; Harris, D. A novel discrete model for granular material incorporating rolling resistance. *Comput. Geotech.* **2005**, *32*, 340–357. [CrossRef]
17. Nitka, M.; Grabowski, A. Shear band evolution phenomena in direct shear test modelled with DEM. *Powder Technol.* **2021**, *391*, 369–384. [CrossRef]
18. Suchorzewski, J.; Tejchman, J.; Nitka, M. Experimental and numerical investigations of concrete behaviour at meso-level during quasi-static splitting tension. *Theor. Appl. Fract. Mech.* **2018**, *96*, 720–739. [CrossRef]
19. Donzé, F.V.; Magnier, S.-A.; Daudeville, L.; Mariotti, C.; Davenne, L. Numerical Study of Compressive Behavior of Concrete at High Strain Rates. *J. Eng. Mech.* **1999**, *125*, 1154–1163. [CrossRef]
20. Hentz, S.; Daudeville, L.; Donzé, F.V. Identification and Validation of a Discrete Element Model for Concrete. *J. Eng. Mech. ASCE* **2004**, *130*, 709–719. [CrossRef]
21. Dupray, F.; Malecot, Y.; Daudeville, L.; Buzaud, E. A mesoscopic model for the behaviour of concrete under high confinement. *Int. J. Numer. Anal. Methods Geomech.* **2009**, *33*, 1407–1423. [CrossRef]
22. Groh, U.; Konietzky, H.; Walter, K.; Herbst, M. Damage simulation of brittle heterogeneous materials at the grain size level. *Theor. Appl. Fract. Mech.* **2011**, *55*, 31–38. [CrossRef]
23. Rangari, S.; Murali, K.; Deb, A. Effect of meso-structure on strength and size effect in concrete under compression. *Eng. Fract. Mech.* **2018**, *195*, 162–185. [CrossRef]
24. Nguyen, T.T.; Bui, H.H.; Ngo, T.D.; Nguyen, G.D.; Kreher, M.U.; Darve, F. A micromechanical investigation for the effects of pore size and its distribution on geopolymer foam concrete under uniaxial compression. *Eng. Fract. Mech.* **2019**, *209*, 228–244. [CrossRef]
25. Krenzer, K.; Mechtcherine, V.; Palzer, U. Simulating mixing processes of fresh concrete using the discrete element method (DEM) under consideration of water addition and changes in moisture distribution. *Cem. Concr. Res.* **2019**, *115*, 274–282. [CrossRef]
26. Nitka, M.; Tejchman, J. Comparative DEM calculations of fracture process in concrete considering real angular and artificial spherical aggregates. *Eng. Fract. Mech.* **2020**, *239*, 107309. [CrossRef]
27. Rojek, J.; Madan, N.; Nosewicz, S. Micro–Macro Relationships in the Simulation of Wave Propagation Phenomenon Using the Discrete Element Method. *Materials* **2019**, *12*, 4241. [CrossRef]
28. Rose, J.L. *Ultrasonic Guided Waves in Solid Media*; Cambridge University Press: New York, NY, USA, 2014; ISBN 9781107273610.
29. Kozicki, J.; Donzé, F.V. A new open-source software developed for numerical simulations using discrete modeling methods. *Comput. Methods Appl. Mech. Eng.* **2008**, *197*, 4429–4443. [CrossRef]
30. Šmilauer, V.; Chareyre, B. Yade DEM Formulation. *Yade Doc.* **2010**, *2011*, 38.
31. Ergenzinger, C.; Seifried, R.; Eberhard, P. A discrete element model to describe failure of strong rock in uniaxial compression. *Granul. Matter* **2011**, *13*, 341–364. [CrossRef]
32. Ng, C.T. On the selection of advanced signal processing techniques for guided wave damage identification using a statistical approach. *Eng. Struct.* **2014**, *67*, 50–60. [CrossRef]
33. Schober, P.; Schwarte, L.A. Correlation coefficients: Appropriate use and interpretation. *Anesth. Analg.* **2018**, *126*, 1763–1768. [CrossRef]
34. Seco, F.; Martín, J.M.; Jiménez, A.; Pons, J.L. PCdisp: A Tool for The Simulation of Wave Propagation in Cylindrical Waveguides. In Proceedings of the 9th International Congress on Sound and Vibration, Orlando, FL, USA, 8–11 July 2002.
35. Seco, F.; Jiménez, A.R. Modelling the Generation and Propagation of Ultrasonic Signals in Cylindrical Waveguides. In *Ultrasonic Waves*; BoD—Books on Demand: Norderstedt, Germany, 2012. [CrossRef]